Chemical Science

ROYAL SOCIETY OF CHEMISTRY

EDGE ARTICLE

View Article Online
View Journal | View Issue

Cite this: *Chem. Sci.*, 2025, **16**, 20851

All publication charges for this article have been paid for by the Royal Society of Chemistry

Crystallization-driven two-dimensional assemblies from a phenothiazine-conjugated poly(L-lactide): redox-responsive tunable emission, white-light harvesting and surface-enabled nanoparticle decoration

Chhandita Chakraborty and Anindita Das *

Crystallization-driven self-assembly (CDSA) of amphiphilic crystallizable block copolymers represents a powerful tool for constructing precision nanostructures with uniform shapes and dimensions. To date, major efforts have been made towards achieving structural control by employing living-CDSA. Herein, we unravel a new approach for precision two-dimensional (2D) architectures that can exhibit redox-responsive surface-emission color tunability, including white-light harvesting from a single phenothiazine end-capped poly(L-lactide) homopolymer (**PTZ-P1**) without compromising the intrinsic 2D morphology. By CDSA in 20% isopropanol/water, **PTZ-P1** produced lozenge-shaped nanoplatelets with multilayered thickness *via* crystallization of the poly(L-lactide) core, while the phenothiazine (PTZ) moieties occupying the 2D surface act as the soluble corona. These surface-bound PTZ units show selective and ratiometric sensing toward hypochlorite ions (ClO^-), a key component of the reactive oxygen species, with a low detection limit of 1.54 μM. The sensing response is triggered by NaClO-induced oxidation of the surface-anchored PTZ to phenothiazine sulfoxide (OPTZ), as confirmed by X-ray photoelectron spectroscopy (XPS) and mass spectrometry data, which alters the emission color of the nanoplatelets from orange to cyan *via* an intermediate white-light-emitting state with CIE coordinates (0.31, 0.36), depending on the analyte concentration. The *in situ* formation of the white-light-emitting platelets was attributed to the partial oxidation of PTZ (orange-emissive) to OPTZ (cyan-emissive) on the 2D surface, as confirmed by confocal microscopy imaging. This yielded a broad-emission spectrum, ranging from 400 to 750 nm, producing white light. Building on this, co-assembly of **PTZ-P1** with its oxidized counterpart, **OPTZ-P1**, separately synthesized from a phenothiazine sulfoxide initiator (**OPTZ-OH**), was successfully achieved for better control over the surface emission properties. At a composition of 7 : 1 (**OPTZ-P1** : **PTZ-P1**), stable white-light-emitting platelets (CIE: 0.31, 0.32) were produced due to the dual color emission and contribution from Förster resonance energy transfer (FRET), with a 32% efficiency between the donor (OPTZ) and acceptor (PTZ) chromophores. In contrast, mixing preformed **PTZ-P1** and **OPTZ-P1** platelets at a 2 : 1 ratio also yielded near-white light *via* only additive color mixing, without FRET, from the spatially separated orange- and cyan-emitting platelets. Interestingly, surface-grafted PTZ moieties enabled photo-induced silver nanoparticle deposition, imparting conductive properties to the **PTZ-P1** nanoplatelets.

Received 16th June 2025
Accepted 26th September 2025

DOI: 10.1039/d5sc04392a

rsc.li/chemical-science

Introduction

Organic two-dimensional (2D) materials[1] have garnered a lot of attention because of their broad potential applications, ranging from photonic and electronic devices[1d–f] to biomaterials.[1g] Among these, two-dimensional self-assembled π-systems[2] have attracted particular interest for their tunable optoelectronic properties covering large surface areas, which play a critical role in determining their functional potential. However, controlling hierarchical supramolecular assembly of π-systems in two dimensions over mesoscopic length scales is a key challenge,[3] largely due to the absence of generally applicable methods that can generate 2D assemblies with structural predictability and uniformity. Crystallization-driven self-assembly (CDSA) of crystallizable block copolymers has gained tremendous attention as a potent method for creating a variety of complex hierarchical anisotropic architectures in the solution phase.[4] This technique enables the core-forming polymeric block to crystallize *via*

School of Applied and Interdisciplinary Sciences, Indian Association for the Cultivation of Science (IACS), 2A and 2B Raja. S. C. Mullick Road, Jadavpur, Kolkata 700032, India. E-mail: psuad2@iacs.res.in

a chain-folding process in a corona-selective solvent, which forces the terminal corona-forming block to locate on the surface of the resultant crystalline lamellae and offer colloidal stability. Furthermore, building on the principles of living/controlled covalent polymerization,[5] living crystallization-driven self-assembly (living-CDSA)[6] has emerged as a powerful strategy that offers precise control over the size, shape, topology, sequence and dispersity of the block copolymer nanostructures, which could be readily achieved by adjusting the unimer: seed ratio and other self-assembly conditions.[7] The possibility for exceptional structural control expands the application of this living-CDSA strategy into broader areas of living supramolecular polymerization of π-systems.[8] In a different approach, we first attempted to integrate CDSA of crystallizable polymers with the self-assembly of π-systems to expand the potential of this technique beyond non-functional block copolymers. In this context, we earlier reported a novel supramolecular bottom–up strategy for creating monolayered 2D assemblies of π-systems from various chromophore-conjugated poly(L-lactide) (PLLA) homopolymers *via* CDSA with predictable morphology and programmable surface properties.[9] By strategically incorporating different corona-forming polar dyes at the chain end of the semicrystalline PLLA homopolymers, we successfully generated well-defined lozenge (diamond)-shaped crystalline lamellae with excellent colloidal stability and fluorescent properties in isopropanol (iPrOH). The ordered 2D array of polar chromophores on the platelet surface enabled effective dispersion in the corona-selective polar solvent through favorable chromophore–solvent interactions, which allowed the crystalline lamellae to achieve the required colloidal stability for discrete monolayered structure formation. This end-group engineering strategy involving the incorporation of different π-systems in place of conventional non-functional polymeric segments remarkably expanded the functional diversity and design scope of the CDSA-derived nanostructures. Additionally, by incorporating appropriate donor–acceptor pairs at the PLLA chain end, Förster resonance energy transfer (FRET) could be achieved from the 2D surface of these polymeric single crystals.[9a,b] Despite these attractive features, CDSA-driven polymeric 2D materials capable of modulating their surface emission properties upon exposure to external stimuli remain largely elusive.[10] Independently, stimuli-responsive π-systems[11] with tunable properties originating from their ability to physically or chemically respond to a variety of external stimuli have drawn significant attention. We envisaged that integrating such responsive π-systems to crystallizable polymers will endow CDSA-based nanostructures with unprecedented surface-tunable optical properties while preserving the structural integrity of the crystalline core. This might pave the way for the design of customizable 2D materials for sensing, detection, and other advanced functions, which remain unexplored in the field of CDSA.

As a proof-of-concept, herein, we designed and synthesized redox-active CDSA-induced 2D nanoplatelets from a phenothiazine (PTZ) dye end-capped PLLA polymer (**PTZ-P1**) (Scheme 1). The sulfur atom in the phenothiazine moiety is in the sulfide state (+2 oxidation) and can be oxidized to sulfoxide (+4 oxidation) and sulfone (+6 oxidation) states[12] in the presence of different reactive oxygen species (ROS), including hypochlorite ions (ClO^-).[12c] The optoelectronic properties of phenothiazine 5-oxide (sulfoxide) and phenothiazine 5,5-dioxide (sulfone) exhibit drastic changes as the electron-donating sulfur (S) atom in the sulfide state transforms into electron-withdrawing sulfoxide/sulfone.[13] Taking advantage of the redox properties of the surface-decorated PTZ dye, we herein demonstrated stimuli-responsive surface modifications of the **PTZ-P1** nanoplatelets in the presence of ClO^- ions in a 20% iPrOH/water mixture. This enables unprecedented tuning of the photophysical (fluorescent) properties of the crystalline 2D lamellae derived from the PLLA biopolymer. By hypochlorite (ClO^-) treatment, we could successfully transform orange emissive 2D platelets to cyan emissive ones by selectively oxidizing the surface-occupied PTZ dyes from sulfide to sulfoxide, without affecting the core-forming crystalline lamellae. By integrating the CDSA properties of **PTZ-P1** with the stimuli-responsive emission color tunability of the surface-decorated PTZ chromophores, we

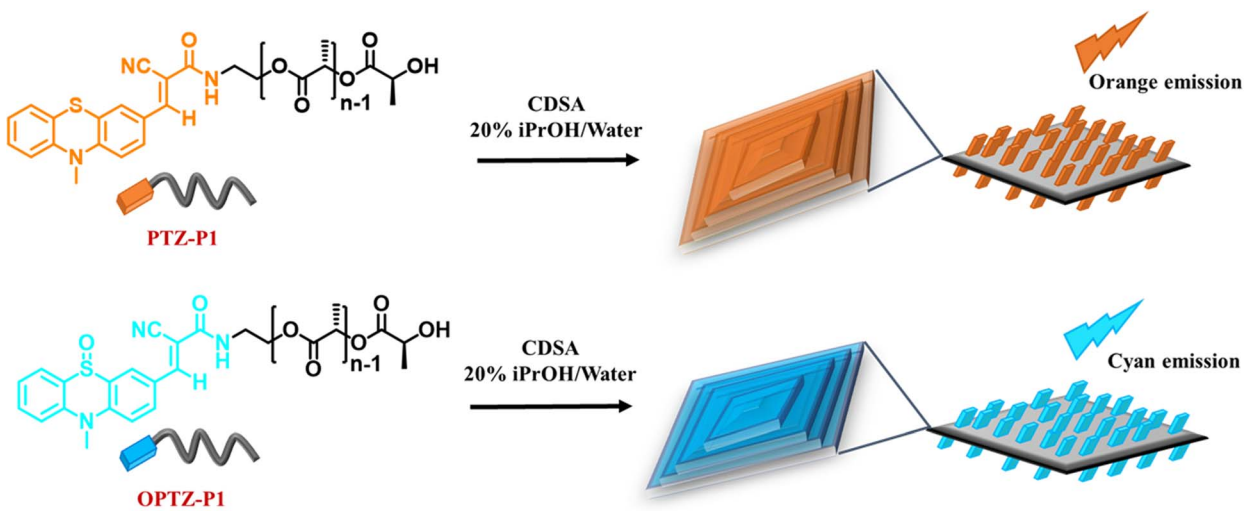

Scheme 1 Schematic illustration of the crystallization-driven self-assembly (CDSA) of PTZ-P1 and OPTZ-P1 in 20% iPrOH/water.

developed a 2D fluorescent probe for the ratiometric detection of ClO^- ions utilizing the fluorescence intensity ratios of the reduced (sulfide) and oxidized (sulfoxide) forms appearing at two independent wavelengths. Noteworthily, the fluorescent color tunability of 2D platelets involves a transient white-light emissive state resulting from the coexistence of complementary orange (sulfide) and cyan (sulfoxide) emissive forms of PTZ within the same platelets during partial oxidation. By optimizing various conditions for partial oxidation of the PTZ moiety, we successfully converted the transient white-light-emitting 2D platelets into a stable form, starting from a single component[14] **PTZ-P1** homopolymer, which is unprecedented in the field of CDSA. Further control over the emission properties of the nanoplatelets was achieved through co-assembly of **PTZ-P1** with its oxidized counterpart **OPTZ-P1**, end-capped with phenothiazine sulfoxide (O-PTZ). Additionally, we explored the role of surface-occupied PTZ in photo-induced silver (Ag) nanoparticle (NP) deposition, where it could function as both a reducing and capping agent by facilitating the formation and/or stabilization of the AgNPs.[15] Unlike the non-conducting nature of the pristine **PTZ-P1** nanoplatelets, the AgNP-decorated counterparts exhibited measurable electrical conductivity, originating from surface-occupied AgNPs.

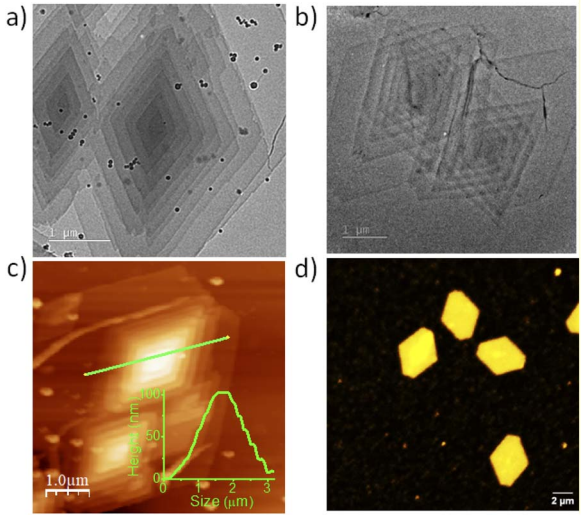

Fig. 1 TEM images of self-assembled **PTZ-P1** exhibiting multi-layered diamond-shaped 2D morphology in (a) iPrOH, $c = 0.25$ mg mL^{-1}; (b) 20% iPrOH/water, $c = 0.05$ mg mL^{-1}; (c) AFM image (inset: showing the height profile of the nanoplatelets) and (d) CLSM image from a solution of **PTZ-P1** in 20% iPrOH/water mixture; $c = 0.05$ mg mL^{-1}. (d) CLSM image from a solution of **PTZ-P1** in a 20% iPrOH/water mixture; $c = 0.05$ mg mL^{-1}.

Results and discussion

Two-dimensional nanostructures by crystallization-driven self-assembly (CDSA) of a phenothiazine-functionalized PLLA homopolymer and its stimuli-responsive tunable fluorescence properties

Phenothiazine (PTZ)-end-capped poly(L-lactide) **PTZ-P1** was synthesized by ring-opening polymerisation (ROP) of the L-lactide monomer using a hydroxyl-functionalized phenothiazine-based initiator (**PTZ-OH**) and reported elsewhere.[9c] Following a similar synthetic procedure, phenothiazine sulfoxide (OPTZ)-conjugated **OPTZ-P1** (Scheme 1) was synthesized from **OPTZ-OH** (see the SI). In order to detect hypochlorite ions, herein, we aimed to achieve 2D assemblies of **PTZ-P1** in an aqueous medium. At first, we generated the 2D platelets from **PTZ-P1** in isopropanol (iPrOH) ($c = 0.25$ mg mL^{-1}) by heating the solution vigorously and then allowing it to cool spontaneously and age for 30 minutes, which produced lozenge- and truncated-lozenge-shaped multi-layered, pyramid-like nanoplatelets with an average size of ≈3 to 3.5 μm, as visualized by transmission electron microscopy (TEM) (Fig. 1a, S1a and b) and atomic force microscopy (AFM) (Fig. S1c and d). The average central thickness of the multi-layered 2D structures was ∼100 nm (Fig. S1d). This is in sharp contrast to our previous report of single-layered 2D platelets from a lower concentration ($c = 0.05$ mg mL^{-1}) of **PTZ-P1** in iPrOH,[9c] with a thickness of ∼8 to 9 nm, nearly equivalent to the length of ∼32 repeating units.[16b,c] Similar concentration effects on the lamellar thickness were previously reported by He and co-workers with the conjugated diblock copolymer, poly(*p*-phenylenevinylene)-*block*-poly(-ethyleneglycol).[16a] They showed a uniform decrease in the lateral dimension with increasing height towards the middle of the 2D assemblies, which was driven by a screw dislocation mechanism.[16a] Next, we gradually dispersed these 2D structures prepared in iPrOH into water to adjust the final solvent composition to 20% iPrOH/water and a concentration of 0.05 mg mL^{-1}. The TEM images of **PTZ-P1** in 20% iPrOH/water (Fig. 1b and S1e–h) revealed the major formation of multi-layered 2D structures with strong interplatelet interactions. The AFM analysis (Fig. 1c and S1i–q) showed a uniform decrease in lateral dimension with a central lamellar thickness of ∼80–100 nm due to screw dislocation, similar to what was observed in iPrOH. The multi-layered 2D structures were strongly facilitated by the increased concentration of **PTZ-P1** in iPrOH[16a] and hydrophobically predominated π–π interactions between the surface-decorated PTZ dyes, which caused additional aggregation propensity in the water-rich environment as evident from the TEM images (Fig. S1e–h). The surface-occupied PTZ chromophores confer good colloidal stability to the resultant 2D platelets as indicated by the lack of visible precipitation in 20% iPrOH/water at the tested polymer concentration. The 2D platelets displayed orange emission from the surface-occupied PTZ dyes, as evident from the confocal laser scanning microscopy (CLSM) images (Fig. 1d). Next, we explored the redox-responsive properties of the resultant 2D platelets by titrating with varying concentrations of NaClO. As shown in Fig. 2a, **PTZ-P1** displayed two absorption bands at 313 and 435 nm in 20% iPrOH/water, which is the characteristic of the end-capped PTZ chromophore. Notably, the **PTZ-P1** absorption band gradually disappeared with a concomitant emergence of a new band centered at $\lambda \sim 390$ nm upon addition of ClO^-. At wavelengths of 344 nm and 417 nm, two different isosbestic sites were observed, which correlated with the transition of the surface-bound PTZ dyes between two different states. Similarly, when **PTZ-P1** was exposed to NaClO, its

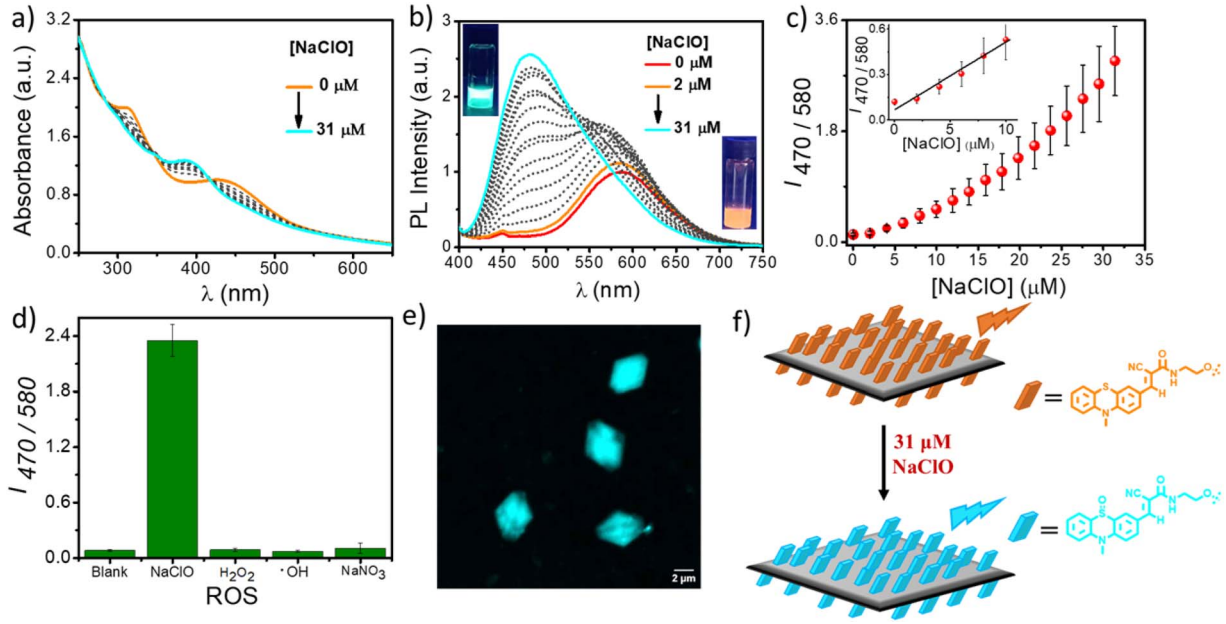

Fig. 2 The changes observed in the (a) absorption spectra of **PTZ-P1** (c = 0.1 mg mL^{-1}) and (b) normalized fluorescence spectra of **PTZ-P1** (c = 0.05 mg mL^{-1}) upon addition of NaClO (0–31 μM); each spectrum was recorded after 3 min in 20% iPrOH/water (λ_{ex} = 390 nm); (c) plot of the fluorescence intensity ratios ($I_{470/580}$) monitored at 470 nm and 580 nm of **PTZ-P1** from the titration plot (b) (inset: $I_{470/580}$ plot showing linear changes upon addition of lower concentrations of NaClO in the range of 1–10 μM); (d) fluorescence response of **PTZ-P1** (c = 0.05 mg mL^{-1}) in the presence of NaClO, ˙OH (Fenton's reagent), H_2O_2 and $NaNO_3$. Emission signals were recorded at 470 nm (λ_{ex} = 390 nm); (e) CLSM image of **PTZ-P1** in 20% iPrOH/water after exposure to NaClO showing a color change from orange to cyan; (f) schematic representation of hypochlorite-triggered emission color tuning properties displayed by **PTZ-P1** nanoplatelets. The actual nanoplatelets are multi-layered; the schematic diagram is simplified by showing single-layered structures.

fluorescence changed from orange to cyan, causing a pronounced blue-shifted emission from 580 to 470 nm (Fig. 2b). As the NaClO concentration increased, the fluorescence intensity at 470 nm clearly increased, and in tandem, the peak at 580 nm declined and eventually vanished. At an NaClO concentration of 31 μM, the fluorescence intensity (λ_{em} = 470 nm) reached a maximum at an excitation wavelength of λ_{ex} = 390 nm, with a 16-fold increment as compared to the initial state (Fig. 2b). This is also visible from the change in the emission color of the solution from orange to cyan upon UV light irradiation ($\lambda_{ex} \sim$ 390 nm) (Fig. 2b inset). Fluorescence intensity ratios ($I_{470/580}$) monitored at 470 nm and 580 nm were used to test **PTZ-P1**'s detection ability for NaClO. The $I_{470/580}$ plot displayed a linear relationship with the concentration of NaClO between 0 and 10 μM (R^2 = 0.81348), with a limit of detection (LOD) of 1.54 μM and a limit of quantification (LOQ) of 5.298 μM using $3\sigma/m$ and $10\sigma/m$ respectively (Fig. 2c),[17] where σ represents the standard deviation of three blank measurements and m is the slope obtained from the graph of the fluorescence intensity ratio *vs.* concentration of NaClO. **PTZ-P1** (c = 0.05 mg mL^{-1}) can therefore detect NaClO in a concentration range of 1.54 μM to 31 μM, significantly lower than the physiological range of hypochlorite (5–200 mM).[18] Next, the sensitivity of **PTZ-P1** to other reactive oxygen species was examined (Fig. 2d). Unlike the prompt and noticeable change observed in the fluorescence properties of **PTZ-P1** as marked by the emergence of the emission band centered at 470 nm when treated with NaClO (c = 30 μM), the interactions with other types of ROS or ROS precursors [H_2O_2, ˙OH (Fenton's reagent) and $NaNO_3$] in a similar concentration range resulted in negligible changes in fluorescence, even after 4 hours of exposure (Fig. 2d). Cyclic voltammetry measurements of all tested ROS generators show that NaClO has the highest reduction potential (0.35 V), making it the strongest oxidizing agent, which possibly renders it capable of selectively oxidizing the electron-rich sulfur atom of phenothiazine under the given experimental conditions (Fig. S2a–g). This demonstrates the high specificity of the **PTZ-P1** platelets for NaClO, making it a promising candidate for hypochlorite sensing. To further test whether such changes in the emission spectra affect the morphology, CLSM imaging was performed on the hypochlorite-treated **PTZ-P1** samples. As shown in Fig. 2e, 2D platelets treated with NaClO (c = 31 μM) displayed a strong cyan emission with the retention of the supramolecular structure, indicating that the NaClO responsiveness is limited to surface property changes as depicted in Fig. 2f. Unlike previously reported stimuli-responsive systems that underwent morphological changes,[19] the structural robustness of the crystalline PLLA core allowed the NaClO-induced changes to be confined exclusively to the surface without affecting the primary 2D crystalline lamellae, making CDSA-induced **PTZ-P1** platelets a robust chemosensor for the real-time detection of hypochlorite ions.

To better comprehend the origin for such hypochlorite sensing by the 2D probe, we subsequently conducted a series of experiments to identify the chemical species formed on the 2D surface that contributed to the observed cyan color emission.

We first identified the reaction product of the initiator, **PTZ-OH**, upon hypochlorite ion (ClO^-) treatment. Following a 30-minute reaction between **PTZ-OH** and NaClO, high-resolution mass spectrometry (HRMS) analysis of the probe revealed prominent mass peaks for [**OPTZ-OH** + H]$^+$ at 368.1165 and for [**OPTZ-OH** + Na]$^+$ at 390.0960, corresponding to the oxidized sulfoxide derivative (**OPTZ-OH**) (Fig. S2h). Consistent with this, NaClO-treated **PTZ-OH** in 20% iPrOH/water exhibited a similar change in the emission color from orange to cyan (Fig. S2i), matching the emission color change observed from the **PTZ-P1** 2D probe (inset Fig. 2b). This finding suggests the oxidation of surface-anchored phenothiazine (PTZ) to phenothiazine sulfoxide (OPTZ) upon exposure to hypochlorite ions, causing cyan colored fluorescence.[20] To further validate this hypothesis, we aimed to directly synthesize cyan-emitting 2D platelets by CDSA from the PLLA homopolymer end-capped with the oxidized initiator (**OPTZ-OH**). We first created **OPTZ-OH** by treating **PTZ-OH** with NaClO at room temperature in acetonitrile, which resulted in controlled oxidation. Subsequent ring-opening polymerization (ROP) of L-lactide using **OPTZ-OH** resulted in a new **OPTZ-P1** homopolymer (Scheme 1), which displayed a degree of polymerization (DP) = 140, and a monomodal size distribution with dispersity ($Đ$) = 1.19, as determined by size exclusion chromatography (SEC) analysis (Fig. S3).

Evidence for the chemical transformation of the surface-decorated PTZ to OPTZ was provided by X-ray photoelectron spectroscopy (XPS) analysis of **PTZ-P1**, **OPTZ-OH**, and **OPTZ-P1** (Fig. 3a and S4). In **PTZ-P1**, the sulfur atom's 2p orbital binding energy (BE) appeared at 164.2 eV, which represents the +2 oxidation state[21] of sulfur and it exhibits the expected spin–orbit doublet (S $2p_{3/2}$ and S $2p_{1/2}$). In contrast, the BE of the sulfur 2p orbital shifted to 168.3 eV in the **OPTZ-P1** polymer (Fig. 3a), matching that of the oxidized **OPTZ-OH** initiator, which corresponds to the +4 oxidation state of sulfur[21] (Fig. S4d), thereby confirming the transformation of phenothiazine (PTZ) to phenothiazine sulfoxide (OPTZ) upon ClO^- treatment. **OPTZ-P1** also produced multi-layered truncated lozenge-shaped platelets in 20% iPrOH/water (Fig. S5a and b), similar in morphology to **PTZ-P1**, and displayed strong cyan emission (Fig. S5c and d). This further establishes that the hypochlorite-triggered oxidation of surface-decorated PTZ to OPTZ caused the change in the emission color of the 2D platelets from orange to cyan (Fig. 2f).

Next, to verify the stability of **OPTZ-P1** in its sulfoxide state, we treated the preformed platelet of **PTZ-P1** in a 20% iPrOH/water mixture with ~52 μM NaClO (saturated equivalent) and monitored the time-dependent changes in the emission properties (Fig. 3b). Within 1 minute, a new emission band at 470 nm corresponding to the sulfoxide was generated along

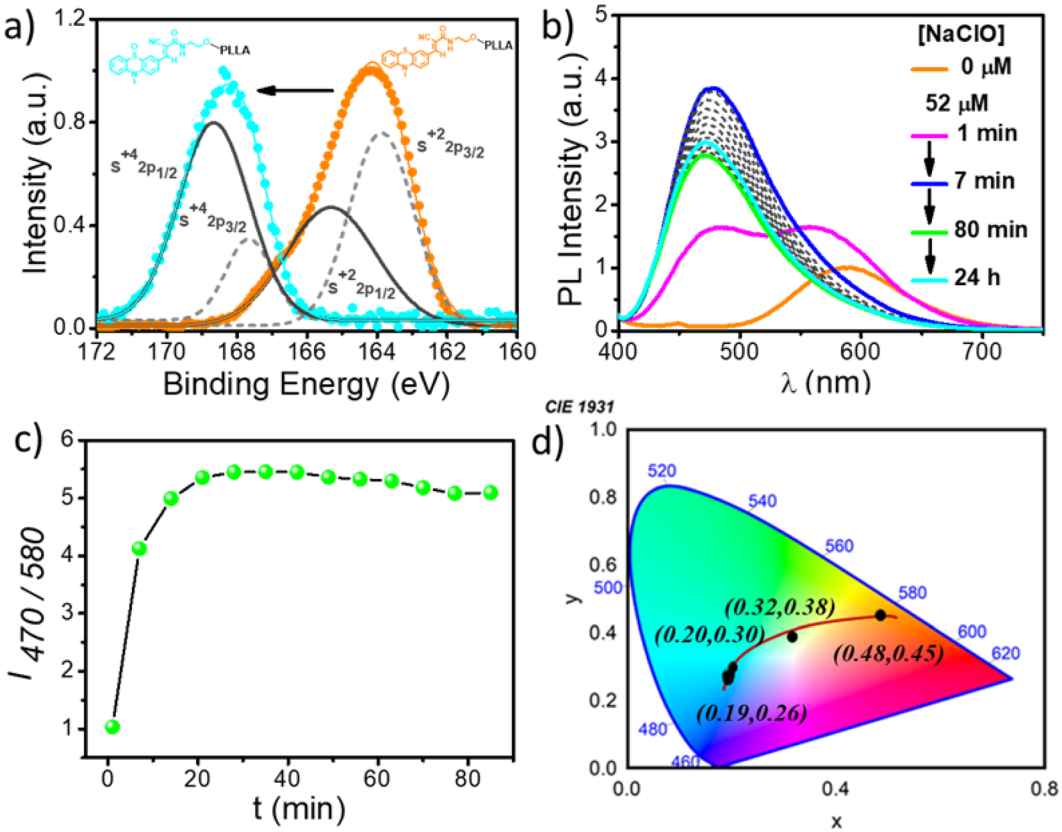

Fig. 3 (a) XPS spectra of the S 2p orbital of **PTZ-P1** (orange trace) and **OPTZ-P1** (cyan trace); (b) the time-dependent changes in fluorescence spectra of **PTZ-P1** in the presence of 52 μM (saturated amount) of NaClO in 20% iPrOH/water (c = 0.05 mg mL^{-1}) monitored up to 24 hours; PL spectra displayed normalized fluorescence intensity; (c) changes in the fluorescence intensity ratios ($I_{470/580}$) monitored at 470 nm and 580 nm plotted as a function of time from (b); (d) luminescent color coordinates obtained from the time-dependent changes in fluorescence spectra of **PTZ-P1** up to 24 h plotted in the Commission Internationale de L'Eclairage (CIE) 1931 chromaticity diagram.

with the original band for PTZ at 580 nm, suggesting partial oxidation. The band corresponding to the reduced (PTZ) form disappeared within 7 minutes with a further increase in the intensity of the new peak at 470 nm. After 20 minutes, the fluorescence intensity ratio ($I_{470/580}$) reached equilibrium and remained unaltered (Fig. 3c). Confocal microscopy images (Fig. S6a and b) clearly showed no loss of structural integrity of the *in situ* formed cyan emissive 2D platelets even after 24 h of NaClO treatment. In fact, even a 7-day aged sample did not show any noticeable change in the morphology or fluorescence properties, indicating the robustness of the 2D structure (Fig. S7a). In agreement, the 2D platelets generated directly from the oxidized polymer, **OPTZ-P1**, showed no change in color or spectral properties over the same tested period of time (Fig. S7b). Thus, **OPTZ-P1** was the only product formed during the oxidation of **PTZ-P1** in the presence of hypochlorite, and no overoxidized product such as sulfone was detected. Interestingly, upon addition of ClO^-, the solution's emission color shifted from orange (CIE: 0.48, 0.45) to cyan (CIE: 0.19, 0.26) through a transient white-light-emitting state (CIE: 0.32, 0.38)[9b,22] shown in Fig. 3d, which is discussed in detail in the following section.

White-light-emitting two-dimensional assemblies from a redox-responsive PLLA homopolymer by CDSA

In recent years, significant efforts have been devoted towards developing organic light-emitting diodes (OLEDs) for a range of display and lighting applications, owing to their flexibility, processibility, superior color quality and color tunability.[22d] Responsive 2D organic materials that exhibit the properties of color generation and tunability are highly sought after for their ability to dynamically modulate emission properties in response to external triggers. Conventional strategies for white-light-emitting OLEDs largely rely on multicomponent systems combining two complementary colored luminescent dyes or three primary colored (red, green, and blue) dyes that cover the whole visible spectrum from 400 to 750 nm. Although rare, more recent advancements have demonstrated the feasibility of white-light luminating systems from unimolecular emitters, which can be constructed by employing monomer/excimer emission, excited-state intramolecular proton transfer, prompt/delayed dual fluorescence, and hybrid fluorescent/phosphorescent systems.[23] It is still challenging to design

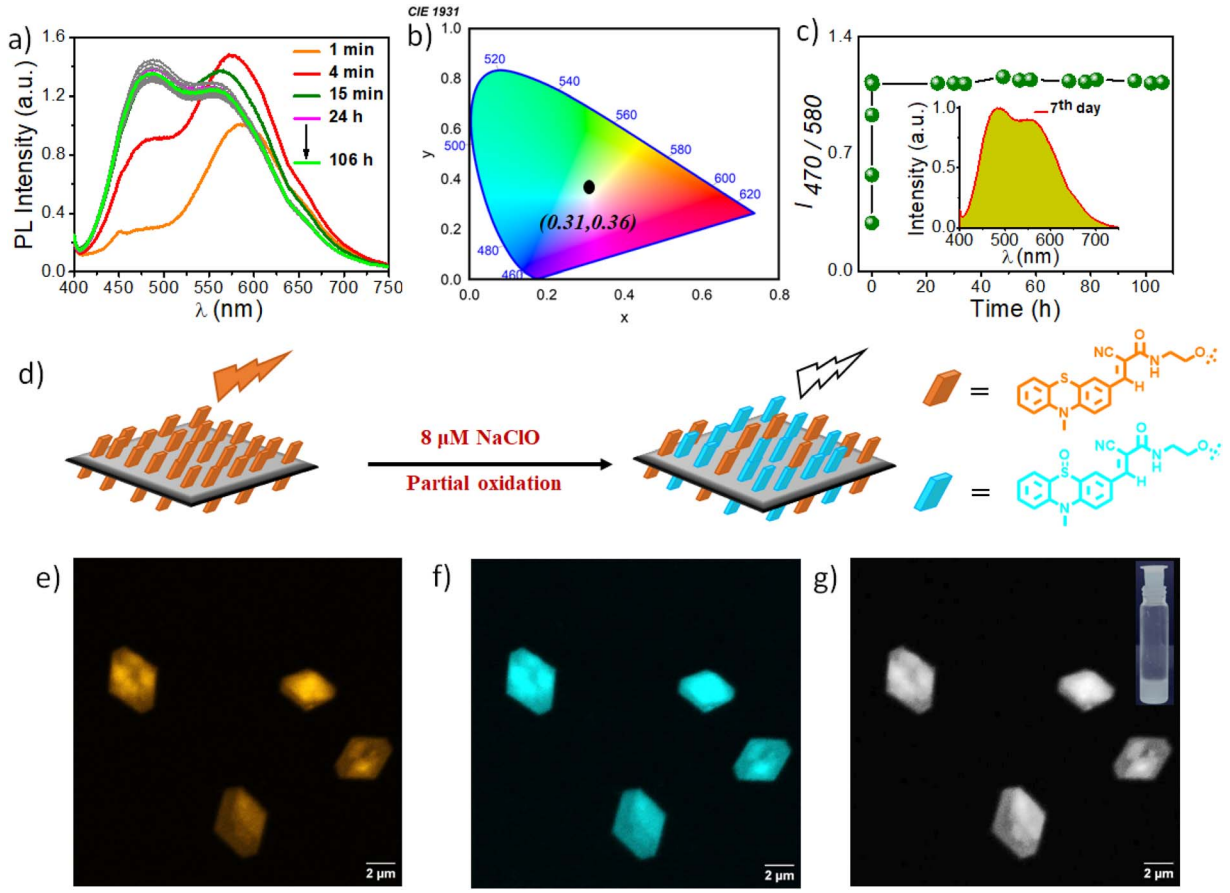

Fig. 4 (a) The time-dependent changes in the fluorescence spectra of **PTZ-P1** ($c = 0.05$ mg mL^{-1}) upon treatment with NaClO (8 μM); PL spectra displayed normalized fluorescence intensity; the broad spectrum generated after 15 minutes remained invariant up to 106 hours and exhibits near-white light as evident from the CIE coordinates of that sample in the (b) CIE 1931 chromaticity diagram; (c) changes in the fluorescence intensity ratios ($I_{470/580}$) monitored at 470 nm and 580 nm of **PTZ-P1** over time as plotted in (a); inset: white-light (WL) emitting spectrum of the same sample on the 7th day; (d) schematic representation of NaClO-triggered transient white-light-emitting 2D nanoplatelets from **PTZ-P1**; CLSM images of NaClO-treated nanoplatelets of **PTZ-P1** visualized through (e) orange channel, (f) cyan channel and (g) without filter showing white-light emission (inset: picture of white-light-emitting solution in 20% iPrOH/water under UV-light irradiation; $\lambda_{ex} = 390$ nm).

single polymeric systems for white-light emission. We previously reported white-light emission through the co-assembly of three separately emissive components (blue, green, and red) *via* crystallization-driven self-assembly (CDSA).[9b] In contrast, we made a significant advancement in this work through the realization of a tunable emission color response from a single-component 2D platelet resulting from the CDSA of **PTZ-P1**. Depending solely on the analyte (ClO^-) concentration, the nanoplatelets of **PTZ-P1** displayed a remarkable change in the emission color from orange to cyan, passing through a transient white-light-emitting state.

Next, to achieve stable white-light emission, we titrated the dispersion of **PTZ-P1** in 20% iPrOH/water with much reduced concentrations of the analyte (8 μM), to prevent complete oxidation. After 15 minutes of ClO^- addition, **PTZ-P1** generated a near-white light emitting broad-spectrum ranging from 400 to 750 nm (Fig. 4a) with CIE coordinates (0.31, 0.36) (Fig. 4b). The emitted white light from the single-component source remained invariant when monitored for up to 7 days (Fig. 4c). The white-light emitting property was attributed to the partial oxidation of the surface-anchored PTZ (orange-emissive) to OPTZ (cyan-emissive) in the presence of ClO^- (Fig. 4d). Therefore, the resulting single-component 2D platelets exhibit dual emission arising from the coexistence of both PTZ and OPTZ chromophores on the 2D surface, with complementary color-emitting properties that generate white light. This was further established by confocal laser scanning microscopy (CLSM) images (Fig. 4e–g), confirming dual cyan and orange emission from the same 2D nanoplatelets, which could be visualized in their respective fluorescence channels (Fig. 4e and f). In the absence of any filter, the resultant platelets emitted white-light (λ_{ex} = 405 nm) (Fig. 4g), and the corresponding solution appeared visibly white under UV light irradiation (λ_{ex} = 390 nm; the inset image of Fig. 4g).

To further validate the white-light emission originating from the simultaneous fluorescence of the complementary color-emitting sulfide (orange) and sulfoxide (cyan) emitters present on the PLLA platelet surface, and also to develop a robust white-light-emitting system, we deliberately co-assembled **PTZ-P1** and **OPTZ-P1**, in different ratios following the CDSA technique in 20% iPrOH/water. **OPTZ-P1**, separately prepared from the oxidized initiator (**OPTZ-OH**), served as the source of the sulfoxide dye, which enabled us to estimate the optimal ratio of oxidized to unoxidized chromophores generated on the 2D surface during the hypochlorite-triggered oxidation. This provides insight into the required compositions of the two chromophores essential for achieving a near-pure white-light-emitting system from a single PLLA homopolymer upon hypochlorite treatment. Among the various compositions tested, the co-assembly of **OPTZ-P1** and **PTZ-P1** in a 7 : 1 ratio produced white-light emitting nanoplatelets with Commission Internationale de l'Éclairage (CIE) coordinates (0.31, 0.32), closely matching with pure white light (Fig. 5a–c). We further investigated the potential contribution of Förster resonance energy

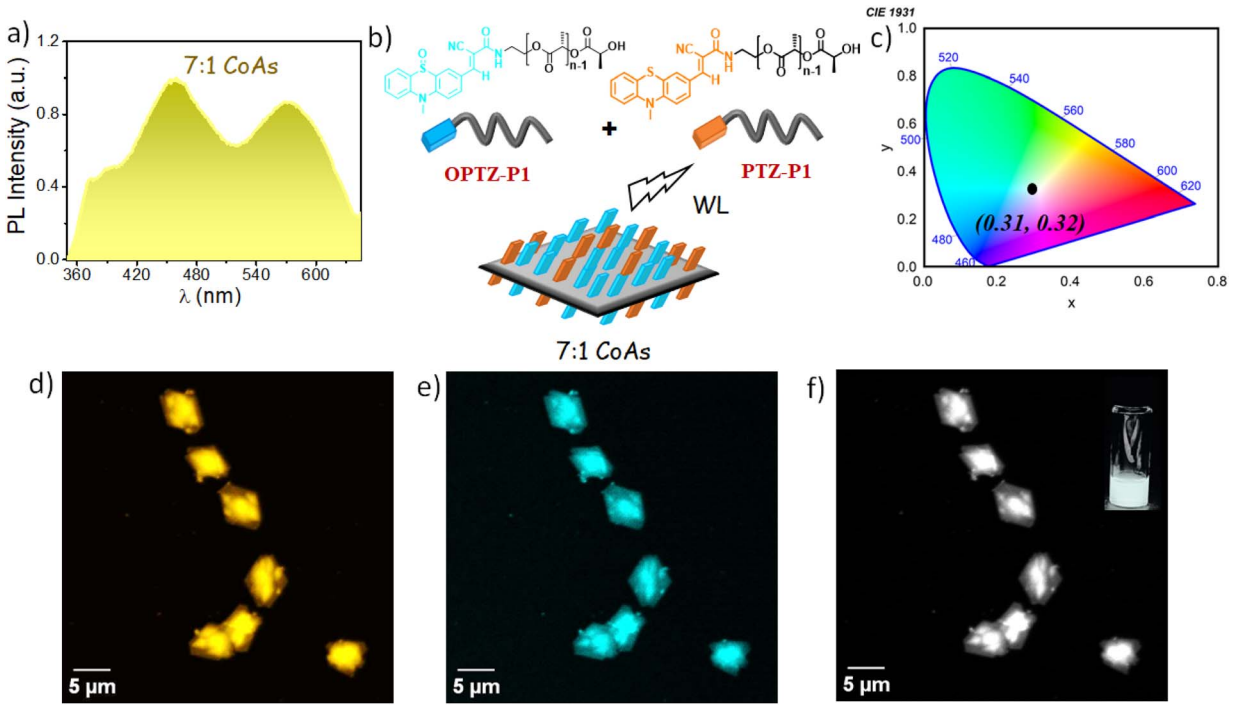

Fig. 5 (a) Normalized photoluminescence (PL) spectrum of the white-light-emitting 2D platelets obtained from a 7 : 1 co-assembly of **OPTZ-P1** (c = 0.14 mg mL^{-1}) + **PTZ-P1** (c = 0.02 mg mL^{-1}) in 20% iPrOH/water; (b) schematic representation of the white-light (WL) emission from the binary co-assembly of **OPTZ-P1** + **PTZ-P1** (7 : 1) by CDSA; (c) near-white-light emitting CIE coordinates obtained from the emission spectrum (taken from (a)) in the CIE 1931 chromaticity diagram; CLSM images showing (d) orange emission, (e) cyan emission and (f) white-light emission in the respective channels, from the 7 : 1 co-assembled 2D platelets (inset: picture of white-light-emitting solution in 20% iPrOH/water under UV-light irradiation; λ_{ex} = 390 nm).

transfer (FRET) between the OPTZ and PTZ chromophores to the overall emission properties and white-light emission. Such possibilities cannot be overruled considering the fact that the two chromophores were colocalized within the permissible FRET range (<10 nm) on the 2D surface.[9,24] Moreover, the sulfoxide (OPTZ) dye could act a potential donor for the sulfide-acceptor (PTZ) with their respective emission and absorbance spectra displaying partial overlap, a prerequisite for FRET. In the 7 : 1 co-assembled system, the time-correlated single-photon counting spectroscopy (TCSPC) measurements revealed a decrease in the fluorescence lifetime of **OPTZ-P1** in the presence of **PTZ-P1** (Fig. S8a and b), indicating the possibility of an intermolecular energy transfer from the OPTZ-donor to the PTZ-acceptor with an estimated FRET efficiency of 32%. While the energy transfer between the OPTZ and PTZ pair was minimal, its role in facilitating white-light emission through spectral broadening from the co-assembled 2D platelets could not be ignored. This was further evident from a control experiment performed with a physical mixture of the preformed 2D platelets of **OPTZ-P1** and **PTZ-P1** that failed to generate white-light in the same 7 : 1 ratio, unlike the co-assembled system (Fig. S8c). This is attributed to the lack of exchange dynamics between the PLLA chains of orange-emitting **PTZ-P1** and cyan-emitting **OPTZ-P1** platelets, resulting in self-sorting. Consequently, the FRET process was suppressed between the spatially separated donor and acceptor chromophores, which is necessary for fine-tuning white-light emission.

Subsequently, we explored the possibility of harvesting white-light from the physical mixture of two complementary color-emitting platelets *i.e.*, **PTZ-P1** and **OPTZ-P1** in a 20% iPrOH/water mixture. Interestingly, a 2 : 1 ratio of the preformed platelets of **OPTZ-P1** and **PTZ-P1** produced white light with CIE coordinates of (0.32, 0.31), closely approaching the ideal white light coordinates (0.33, 0.33) (Fig. 6a–c). Furthermore, the broad emission spectrum generated from the 2 : 1 physical mixture of the 2D assemblies of **OPTZ-P1** and **PTZ-P1** closely resembled the mathematical summation of the individual fluorescence spectra of **OPTZ-P1** and **PTZ-P1** in a 20% iPrOH/water mixture (Fig. 6a). This confirms that no energy transfer occurs between spatially separated cyan- and orange-emitting 2D platelets. In agreement, CLSM imaging displayed self-sorted cyan- and orange-emissive platelets co-localised in the mixture (Fig. 6f), which visibly emitted white-light under UV irradiation (Fig. 6f, inset: solution picture emitting white light). Therefore, the observed white-light emission from the 2 : 1 mixture results from pure additive emission color mixing, unlike in the 7 : 1 co-assembled system where the contribution from FRET in tuning the emission color was also considered. The 7 : 1 co-assembly and 2 : 1 physical mixture of the self-segregated 2D assemblies of **OPTZ-P1** and **PTZ-P1** in the film state (prepared by drop-casting samples from 20% iPrOH/water onto quartz plates and subsequent drying) also produced emission close to white light with CIE coordinates of (0.28, 0.35) and (0.27, 0.34),

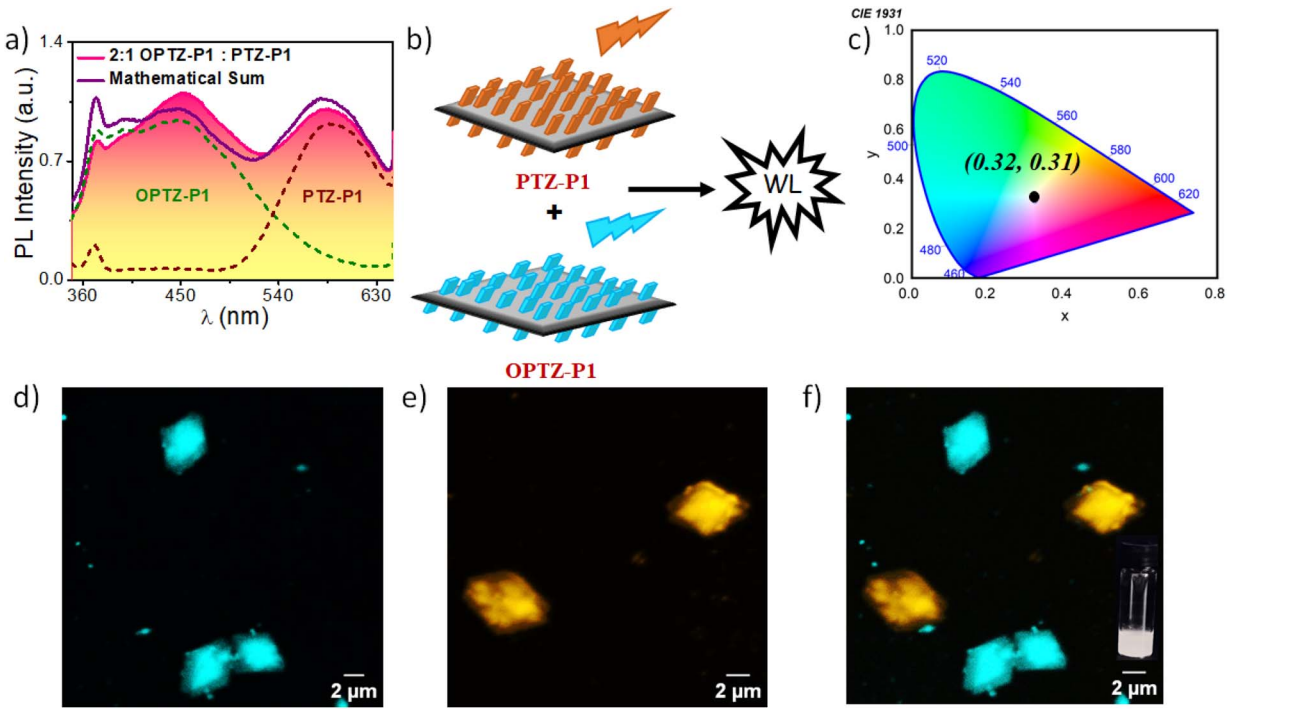

Fig. 6 (a) Comparison of normalized emission spectra of the white-light-emitting 2D platelets obtained from a 2 : 1 self-segregated system of OPTZ-P1 (c = 0.04 mg mL^{-1}) and PTZ-P1 (c = 0.02 mg mL^{-1}) with the mathematical summation of the individual spectra of OPTZ-P1 and PTZ-P1 in 20% iPrOH/water; (b) schematic representation of white-light (WL) emission from 2 : 1 self-segregated 2D assemblies of OPTZ-P1 and PTZ-P1; (c) CIE 1931 chromaticity diagram showing near-white-light CIE coordinates from a 2 : 1 self-segregated system of OPTZ-P1 + PTZ-P1; corresponding CLSM images of the sample showing (d) cyan-emitting platelets and (e) orange-emitting platelets in the respective channels, and their (f) merged image displaying self-sorting; (f) inset: picture of white-light-emitting solution in 20% iPrOH/water (under UV-light-irradiation; λ_{ex} = 390 nm) from self-segregated 2D platelets of OPTZ-P1 and PTZ-P1.

respectively (Fig. S8d–i), indicating their potential as solid-state emitters.

Silver nanoparticle (AgNP)-decorated 2D assemblies and their conducting properties

Because of their intriguing optical properties and possible uses, nanoparticles (NPs) have garnered a lot of interest.[25] More recently, CDSA has established itself as a unique technique for grafting metal nanoparticles onto two-dimensional surfaces, enabling the fabrication of large-area mono-layered assemblies of nanoparticles.[26] Such templated organization of NPs in two-dimensions is anticipated to show emergent properties through plasmonic coupling or quantum effects,[27] as compared to isolated NPs, and therefore, this strategy holds great scientific and technological importance for advancing the scope of functional 2D materials. It is commonly recognised that silver (Ag) nanoparticles (AgNPs) are stabilised by thiol and amine-based ligands *via* Ag–S and Ag–N interactions.[28] Derivatives of phenothiazine are reported to stabilise AgNPs by coordinating with the nitrogen (N) or sulfur (S) sites found in their structures.[15] As the sulfur atom in the phenothiazine (PTZ) moiety is susceptible to oxidation, PTZ chromophores can also be used as mild reductants for the synthesis of inorganic nanoparticles.[28] Using a pulsed laser ablation approach, K. Chandrasekharan *et al.* reported the synthesis of an organo-metallic hybrid system of phenothiazine (PTZ)–silver (Ag), in which PTZ functions as both a stabiliser and a reductant.[15c] Zhu *et al.* conducted a thorough investigation to analyse the capacity of phenothiazine dyes to photochemically produce electrons for the reduction of $AgNO_3$ to AgNPs.[15d]

It is envisaged that upon crystallization of **PTZ-P1**, the chain end-functionalized PTZ moiety, excluded onto the surface of the PLLA crystalline lamellae can trap silver (Ag) nanoparticles and produce AgNP-ornamented 2D surfaces. To realize such possibilities, we followed two approaches. In the first approach, by photo-exciting **PTZ-P1** in 20% iPrOH/water, we successfully created AgNP-decorated 2D surfaces, where phenothiazine served as both a capping and reducing agent. In another approach, we synthesized AgNPs using tetrabutylammonium borohydride (TBAB) as an external reducing agent and explored the capping ability of the PTZ-decorated 2D platelets of **PTZ-P1** as the sole template. A schematic representation of the formation of AgNP-decorated 2D platelets from **PTZ-P1** following both these procedures is illustrated in Scheme 2. In the first method (Scheme 2a), a preformed 2D assembly of **PTZ-P1** ($c = 0.05$ mg mL^{-1}) in 20% iPrOH/water was mixed with a 0.5 μM aqueous solution of $AgNO_3$ and irradiated for 10 minutes with a 427 nm LED bulb (12 W). The formation of the nanoparticles was characterized by TEM imaging. Fig. 7a illustrates the low-magnification TEM image of multi-layered PLLA single crystals. Upon closer inspection of their magnified images at higher resolution (Fig. 7b), the presence of spherical AgNPs grafted on the platelet surface was revealed. According to a statistical analysis of the particle size distribution (Gaussian-fitted histogram), the AgNP size ranges from 2 to 10 nm, with a crest centered at 5.03 nm[29] (inset of Fig. 7b). Through the photoexcitation approach, the resultant 2D assemblies showed strong aggregation, most likely due to AgNPs interacting with adjacent platelets through the surface-occupied PTZ acting as both the reducing and capping agent. The reduction of $AgNO_3$ to AgNPs was accompanied by the partial oxidation of PTZ to OPTZ on the 2D surface, as confirmed by UV-vis and fluorescence spectroscopy upon 10 minutes of UV irradiation ($\lambda_{ex} = 427$ nm, Fig. S9a and b). To ensure that the surface-bound PTZ could act as a capping agent, the PTZ concentration was kept 10 times higher than that of $AgNO_3$ so that excess PTZ was still available for capping the resulting AgNPs on the 2D surface.

Furthermore, elemental analysis of the resultant **PTZ-P1**–Ag hybrid system was conducted by energy dispersive X-ray (EDX) spectroscopy. The EDX spectrum (Fig. 7c) displayed distinctive peaks for carbon, nitrogen, oxygen, sulfur, and silver, indicating the formation of the Ag-functionalized hybrid structure.[15] The corresponding selected-area electron diffraction (SAED) pattern (Fig. 7d) of the AgNPs obtained from Fig. 7b reflects their highly crystalline nature, supporting the findings from the wide-angle

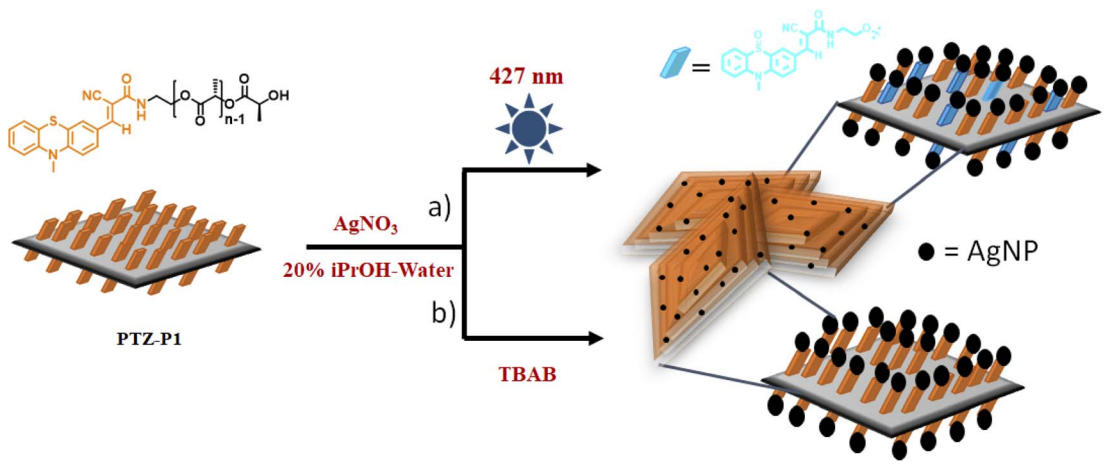

Scheme 2 Schematic representation of the AgNP grafting on PTZ-appended 2D platelets by (a) photo-irradiation and (b) using tetrabutylammonium borohydride (TBAB) as an external reducing agent.

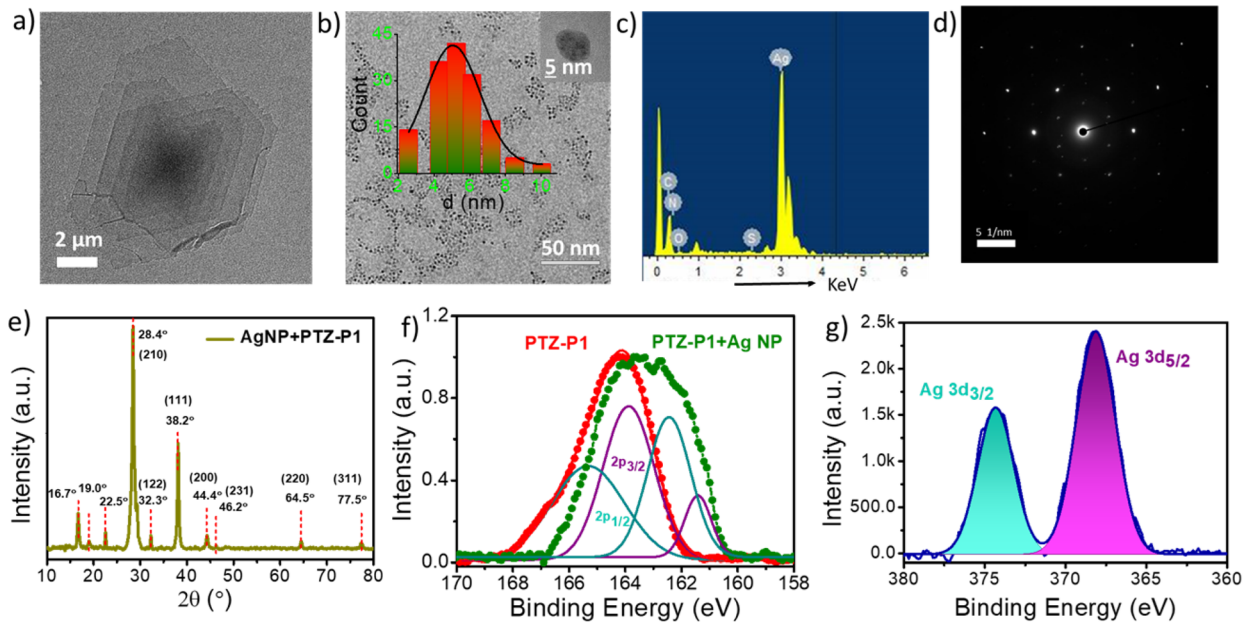

Fig. 7 (a) TEM image of AgNP-grafted **PTZ-P1** 2D nanoplatelets and (b) high-resolution magnified TEM image of (a) showing AgNPs deposited on the 2D surface (inset: histogram of the nanoparticle's size distribution from the TEM image); (c) energy-dispersive X-ray (EDX) spectrum of AgNP-grafted 2D platelets and (d) corresponding SAED pattern of the AgNPs (scale bar: 5 nm^{-1}); (e) WAXD patterns obtained from a thin film prepared by drop-casting a dispersion of AgNP-grafted PLLA platelets from 20% iPrOH/water; (f) XPS data showing shift in the binding energy of the S 2p orbital of **PTZ-P1** after nanoparticle deposition; and (g) corresponding XPS curve fitting of the Ag 3d photoelectron spectrum for Ag nanoparticles stabilized on the **PTZ-P1** 2D surface by Ag–S bonding. The value indicates the elemental form of Ag.

X-ray diffraction (WAXD) analysis of the thin film prepared by solvent drop-casting from 20% iPrOH/water. The XRD pattern of the AgNP-decorated 2D assembly of **PTZ-1** (Fig. 7e) showed diffraction peaks corresponding to 2θ values of 28.4°, 32.3°, 38.2°, 44.4°, 46.2°, 64.5° and 77.5°, indexed as (210), (122), (111), (200), (231), (220) and (311) planes of silver in the face-centered cubic structure (JCPDS, file no. 04-0783),[29] besides the characteristic peaks for the α-form of PLLA crystals[9,30] at 16.7° (110/200), 19.0° (203), and 22.4° (015). This suggests that the structural integrity of the crystalline lamella of PLLA was not compromised during nanoparticle formation, thereby establishing its role as a robust template for NP decoration. From thermo-gravimetric analysis (TGA)[29c,d] 1.8% AgNP loading was observed on 2D platelets (Fig. S9c).

Subsequently, we prepared AgNP-decorated 2D platelets using externally added tetrabutylammonium borohydride (TBAB) as the reducing agent and PTZ-appended 2D platelets as the nanoparticle grafting template (Scheme 2b). To the pre-formed 2D platelets made from 0.05 mg per mL **PTZ-P1** in 20% iPrOH/water, 0.5 μM $AgNO_3$ and 20 μM TBAB were added. The mixture was then left for 40 minutes. The formation of the nanoparticles was characterized by TEM analysis (Fig. S10a–d), which displayed similar results to those obtained for AgNP preparation by the photoexcitation method. The Gaussian-fitted histogram of the particle's size distribution also showed spherical AgNPs decorated on the 2D surface with an average size of ~6 nm (Fig. S10c). The chemical surface analysis was performed by using X-ray photoelectron spectroscopy (XPS) to confirm the interaction between S and N atoms of the PTZ moiety and AgNPs. The binding energy value of S $2p_{3/2}$ showed a shift from 164.2 eV to 161.5 eV (Fig. 7f), which indicates that the chemical environment of the S atoms changed during NP formation as expected during its covalent bonding with the metal nanoparticle.[28a,31a] Furthermore, Fig. 7f shows that the S 2p spectrum of AgNP-decorated 2D platelets has contributions from both unbound S atoms (56%) and AgNP-coordinated S atoms (44%). Considering the fact that the PTZ concentration was taken 10 times in excess of the $AgNO_3$ salt, the presence of free PTZ ligands on the 2D surface is not surprising. Previous studies have shown that phenothiazine can coordinate with the AgNPs through both the sulfur and nitrogen sites, so we also compared the binding energy values of PTZ's N 1s orbital before and after NP formation from the XPS analysis (Fig. S11b).[21b] No significant shift was observed, probably due to the presence of the bulky methyl group on the nitrogen atom and also due to its higher electronegativity than sulfur. Additionally, in the XPS spectrum of AgNP-decorated 2D platelets, two characteristic peaks were observed at 368.2 eV and 374.4 eV, ascribed to the Ag 3d orbital's Ag $3d_{5/2}$ and Ag $3d_{3/2}$ components, respectively (Fig. 7g). On the basis of the peak position, it can be concluded that silver was present in its elemental form [Ag(0)] in the sample.[15b,31b] We also tried to graft AgNPs onto 2D platelets originating from **OPTZ-P1** in the presence of an external reducing agent to investigate the capping potential of the oxidized form of the phenothiazine dye (OPTZ). The sulfur atom in the OPTZ moiety is in a +4-oxidation state, which significantly reduced the ability of the OPTZ-decorated 2D platelets to effectively coordinate with AgNPs, as confirmed by the XPS data (Fig. S12b). The BE of the S 2p orbital of OPTZ did not show any notable shift after AgNP binding. The TEM images revealed the

formation of bigger AgNPs with an average size of ~12 nm along with larger clusters and highly aggregated polymer sheets (Fig. S13a–e). This is in sharp contrast to the distinct lozenge-shaped morphology of the PLLA 2D crystals of **PTZ-P1**, which was preserved after AgNP binding (Fig. 7a). Possibly, the weak interaction between the nanoparticles and the **OPTZ** ligand led to the formation of Ag-nanoparticle clusters with poor colloidal stability, which subsequently destabilized the polymer template. Thus, the OPTZ-decorated 2D assembly was not an effective template for NP grafting. In contrast, the **PTZ-P1** polymer could generate more uniform AgNP-doped 2D platelets through stronger Ag–S coordination with the surface-functionalized PTZ dye, thereby maintaining a better morphological control over its 2D structure.

The conducting nature of AgNPs provides an opportunity for assessing the conducting properties of the otherwise insulating PLLA 2D platelets of **PTZ-P1** when decorated with AgNPs on the surface. An attractive method for characterising electrical properties at the nanoscale is scanning probe microscopy,[32] specifically conductive atomic force microscopy (C-AFM). To obtain surface information, AFM typically uses a micro-fabricated cantilever with a sharp tip. In C-AFM, an electrode is placed at a fixed point on the sample using a conductive cantilever, as shown in Fig. 8a. The current that results from applying a voltage between the electrode and the conductive probe is recorded after the probe has been scanned across a surface. The ability to separate the force feedback, which regulates the tip height, from the current feedback makes it possible to analyze both the electrical conductivity and surface topography at the same time. Using a Pt-coated Si tip, local conductivity measurements on the 2D surface of **PTZ-P1** 2D platelets from drop-cast samples on silicon wafers were performed vertically (out-of-plane) with and without AgNP grafting. Static *I–V* characteristics and correlated current maps with topography were used to comprehensively study the conducting properties of the 2D surfaces. Even at high bias voltages, the 2D current mapping demonstrated that PLLA 2D platelets without AgNP grafting remained insulating as no measured currents were found using C-AFM analysis (Fig. 8c) from the PLLA platelet surfaces (Fig. 8b). In contrast, the contact mode topography and current mapping (V_B = +10 V) data on 2D platelets of AgNP-decorated **PTZ-P1** (prepared using TBAB as a reducing agent) showed a notable current signal at the AgNP sites (Fig. 8d and e). By comparing the current–voltage (*I–V*) curves acquired from the 2D surface (Fig. 8f), a clear illustration of the impact of the silver nanoparticles on the conductive nature of the nanoparticle-ornamented 2D surface was revealed. The bias voltage was scanned from −5 V to +5 V in order to obtain the *I–V* curve. Without AgNPs, the observed current from the PLLA platelet surfaces was almost zero (Fig. 8f). On the other hand, the *I–V* curve from the AgNP-decorated 2D platelets of **PTZ-P1** revealed a significant rise in the current starting at an applied voltage of ~1.5 V, reaching a maximum of 20 nA at a bias voltage (V_B) of 1.9 V (Fig. 8f) above which it became saturated. This illustrates the critical role of surface-grafted AgNPs in conferring electrical conductivity to the PLLA-derived 2D platelets generated by CDSA.

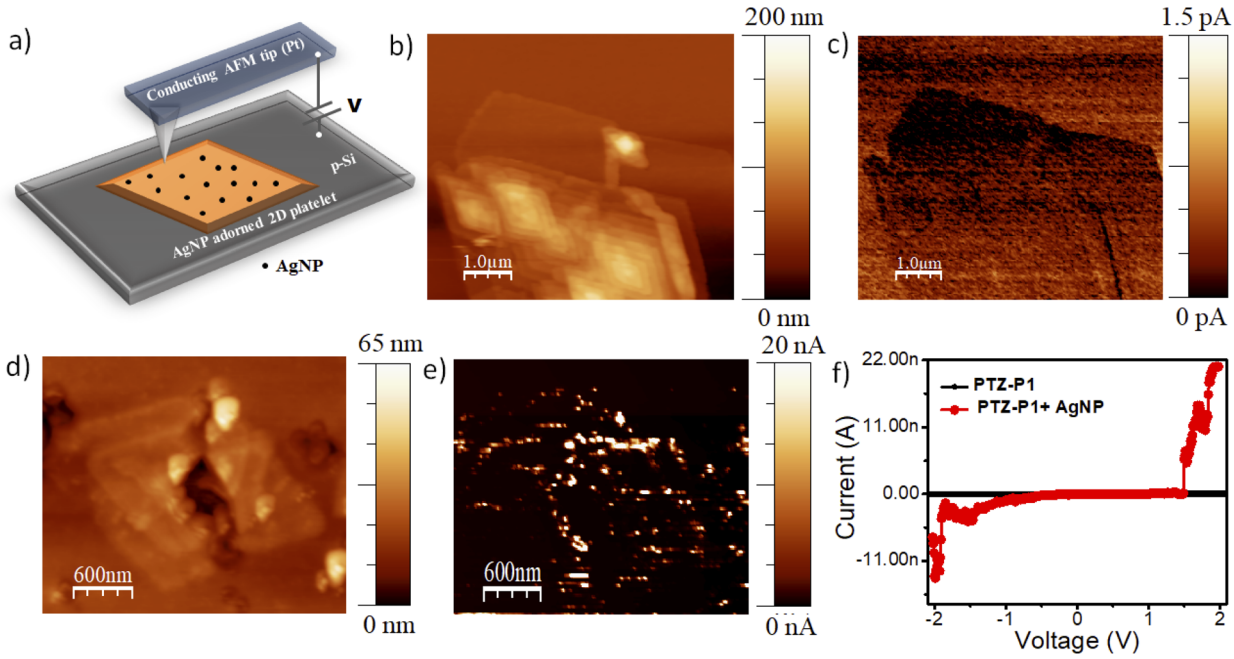

Fig. 8 (a) Schematic representation of the conductive (C)-AFM for electron transport measurement across **PTZ-P1** 2D platelets deposited on a conductive substrate (p-Si) and the AFM tip served as the top electrode, ensuring vertical current measurement. Voltage sweeps from 0 V up to ±10 V were applied to the substrate (with the tip grounded), and the current through the sample was simultaneously measured. The *I–V* measurements were carried out with 20 nA current compliance; topography and current map (C-AFM substrate bias: +10 V) for (b and c) pristine **PTZ-P1** 2D platelets and (d and e) after AgNP deposition on the 2D surface; (f) representative current–voltage (*I–V*) curves obtained from pristine **PTZ-P1** 2D platelets (black trace) and after AgNP deposition (red trace).

Conclusions

In summary, we successfully demonstrated a strategy for redox-active precision two-dimensional (2D) nano-assemblies with tailorable surface-emission properties from a crystallizable phenothiazine end-capped poly(L-lactide) (**PTZ-P1**) homopolymer. By employing the crystallization-driven self-assembly (CDSA) approach, multi-layered lozenge-shaped 2D nanoplatelets were generated in a water-rich medium (20% isopropanol in water). Unlike conventional CDSA strategies that rely on crystallizable block copolymers, where the surface is mostly grafted with a nonfunctional polymeric segment, we judiciously incorporated a redox-active phenothiazine (PTZ) chromophore at the polymer chain end, which not only acts as the surface-occupying corona segment but, being redox active, is additionally able to respond to reactive oxygen species. As a proof-of-concept, we explored the ratiometric fluorescence response of the 2D assembly for hypochlorite ions (ClO^-), which oxidize the surface-grafted PTZ from sulfide to sulfoxide. This chemical transformation was accompanied by a change in emission color from orange to cyan, passing through a transient white-light emitting state, all from a single component system, which is unprecedented in CDSA. Noteworthily, the redox transformation affects only the surface chemistry, preserving the structural features of the core-forming nanoplatelets. Detailed control experiments using a preformed co-assembly of **PTZ-P1** polymer with its oxidized (phenothiazine sulfoxide) counterpart (**OPTZ-P1**) clarified the origin for this white-light emission, which stemmed from the co-localization of the PTZ (orange-emitting) and OPTZ (cyan-emitting) chromophores on the 2D surface during partial oxidation. Furthermore, co-assembly of **OPTZ-P1** and **PTZ-P1** polymers in a specific ratio (7 : 1) yielded stable near-white-light-emitting 2D platelets (CIE 0.31, 0.32) through the contribution of Förster resonance energy transfer (FRET) from surface-occupied OPTZ to PTZ. In contrast, physical mixing of the preformed cyan- and orange-emitting nanoplatelets (2 : 1) produced a white-light-emitting system through simple additive color mixing, without FRET; as a result, the individual platelets could retain their original color. Finally, surface-anchored PTZ moieties were shown to facilitate the photo-induced deposition of Ag nanoparticles (AgNPs), imparting surface-induced electrical conductivity, thereby showing the additional functional benefit of the PTZ-end-capped PLLA nanoplatelets. Overall, this work illustrates a highly versatile 2D system that enables modulating the surface-emission color (including white light) and selective ROS detection, as well as supports surface-induced nanoparticle deposition for conductivity, all from a single-component chromophore-conjugated PLLA homopolymer following a simple CDSA strategy. This strategy offers enormous possibilities for the precise modulation of optical properties through selective surface engineering, showcasing the versatility and robustness of this system. The findings of this work will remarkably broaden the scope of CDSA beyond shape and dimensional control, offering new avenues for the design of functional 2D nanomaterials with surface-induced stimuli-responsive properties.

Author contributions

CC carried out the synthesis and characterization of the polymers, conducted all the experiments and analyzed the data. AD conceptualized the project, raised research funding, and supervised the entire work. The manuscript was written through contributions of all authors. All authors have approved the final version of the manuscript.

Conflicts of interest

There are no conflicts to declare.

Data availability

The data supporting this article have been included as part of the supplementary information (SI). Supplementary information is available. See DOI: https://doi.org/10.1039/d5sc04392a.

Acknowledgements

CC thanks UGC-India for the fellowship. AD thanks BRNS, DAE (grant no. 58/20/10/2022-BRNS/37054), ANRF-SERB CRG (grant no. CRG/2022/003069), and the Technical Research Centre (TRC) of the Indian Association for the Cultivation of Science (IACS) for financial support. The authors thank the Central Scientific Services (CSS) at IACS for the instrumental facilities, Dr Bikash Das (IACS) for assistance in analyzing the C-AFM data and Mr Praduman Kumar Gupta (IACS) for helping with the CV measurements.

Notes and references

1 (*a*) I. Insua, J. Bergueiro, A. Méndez-Ardoy, I. Lostalé-Seijo and J. Montenegro, *Chem. Sci.*, 2022, **13**, 3057; (*b*) A. D. Merg, E. van Genderen, A. Bazrafshan, H. Su, X. Zuo, G. Touponse, T. B. Blum, K. Salaita, J. P. Abrahams and V. P. Conticello, *J. Am. Chem. Soc.*, 2019, **141**, 20107; (*c*) R. R. Liang, S. Y. Jiang, R. Han A and X. Zhao, *Chem. Soc. Rev.*, 2020, **49**, 3920; (*d*) M. C. Lemme, D. Akinwande, C. Huyghebaert and C. Stampfer, *Nat. Commun.*, 2022, **13**, 1392; (*e*) F. Yang, S. Cheng, X. Zhang, X. Ren, R. Li, H. Dong and W. Hu, *Adv. Mater.*, 2018, **30**, 1702415; (*f*) A. Schneemann, R. Dong, F. Schwotzer, H. Zhong, I. Senkovska and X. Feng, *Chem. Sci.*, 2021, **12**, 1600; (*g*) X. Zhang, C. Gong, O. U. Akakuru, Z. Su, A. Wu and G. Wei, *Chem. Soc. Rev.*, 2019, **48**, 5564; (*h*) C. Qian and X. Zhao, *Acc. Chem. Res.*, 2025, **58**, 1192; (*i*) S. Dinda, M. Konar and T. Govindaraju, *Chem. Mat.*, 2024, **36**, 6651; (*j*) C. E. Boott, A. Nazemi and I. Manners, *Angew. Chem., Int. Ed.*, 2015, **54**, 13876.

2 (*a*) C. M. Atienza and L. Sánchez, *Chem.–Eur. J.*, 2024, **30**, e202400379; (*b*) S. Ghosh, D. S. Philips, A. Saeki and A. Ajayaghosh, *Adv. Mater.*, 2017, **29**, 1605408; (*c*) F. Su, Y. Hong, G. Zhang, K. Wu, J. Kim, Z. Chen, H.-J. Zhang and D. Kim, *Chem. Sci.*, 2024, **15**, 5604; (*d*) A. Mukherjee, T. Sakurai, S. Seki and S. Ghosh, *Langmuir*, 2020, **36**,

13096; (*e*) D. Cappelletti, M. Barbieri, A. Aliprandi, M. Maggini and L. Đorđević, *Nanoscale*, 2024, **16**, 9153; (*f*) S. Ghorai, S. Show and A. Das, *Angew. Chem., Int. Ed.*, 2025, **64**, e202500879; (*g*) Z. Gao, J. Sun, L. Shi, W. Yuan and W. Tian, *Chem. Sci.*, 2025, **16**, 8861.

3 (*a*) A. Chakraborty, G. Ghosh, D. S. Pal, S. Varghese and S. Ghosh, *Chem. Sci.*, 2019, **10**, 7345; (*b*) S. Dhiman, R. Ghosh, S. Sarkar and S. J. George, *Chem. Sci.*, 2020, **11**, 12701; (*c*) L. Kleine-Kleffmann, A. Schulz, V. Stepanenko and F. Würthner, *Angew. Chem., Int. Ed.*, 2023, **62**, e202314667; (*d*) P. Khanra, P. Rajdev and A. Das, *Angew. Chem., Int. Ed.*, 2024, **63**, e202400486; (*e*) G. Das, S. Cherumukkil, A. Padmakumar, V. B. Banakar, V. K. Praveen and A. Ajayaghosh, *Angew. Chem., Int. Ed.*, 2021, **60**, 7851; (*f*) N. Sasaki, J. Yuan, T. Fukui, M. Takeuchi and K. Sugiyasu, *Chem.–Eur. J.*, 2020, **26**, 7840; (*g*) N. Sasaki, J. Kikkawa, Y. Ishii, T. Uchihashi, H. Imamura, M. Takeuchi and K. Sugiyasu, *Nat. Chem.*, 2023, **15**, 922; (*h*) M. Kawaura, T. Aizawa, S. Takahashi, H. Miyasaka, H. Sotome and S. Yagai, *Chem. Sci.*, 2022, **13**, 1281.

4 (*a*) J. Massey, K. N. Power, I. Manners and M. A. Winnik, *J. Am. Chem. Soc.*, 1998, **120**, 9533; (*b*) X. Wang, G. Guerin, H. Wang, Y. Wang, I. Manners and M. A. Winnik, *Science*, 2007, **317**, 644; (*c*) F. Teng, B. Xiang, L. Liu, S. Varlas and Z. Tong, *J. Am. Chem. Soc.*, 2023, **145**, 28049; (*d*) S. Mei, M. Staub and C. Y. Li, *Chem.–Eur. J.*, 2020, **26**, 349; (*e*) C. Zhu and J. Nicolas, *Biomacromolecules*, 2022, **23**, 3043; (*f*) W. Xu, Y. Zheng and P. Pan, *J. Polym. Sci.*, 2022, **60**, 2136; (*g*) C. Yang, Z.-X. Li and J.-T. Xu, *J. Polym. Sci.*, 2022, **60**, 2153; (*h*) B. É. Petit, B. Lotz and J. F. Lutz, *ACS Macro Lett.*, 2019, **8**, 779.

5 R. B. Grubbs and R. H. Grubbs, *Macromolecules*, 2017, **50**, 6979.

6 (*a*) S. Ganda and M. H. Stenzel, *Prog. Polym. Sci.*, 2020, **101**, 101195; (*b*) L. MacFarlane, C. Zhao, J. Cai, H. Qiu and I. Manners, *Chem. Sci.*, 2021, **12**, 4661; (*c*) J. Ma, G. Lu, X. Huang and C. Feng, *Chem. Commun.*, 2021, **57**, 13259.

7 (*a*) Y. Cha, C. Jarrett-Wilkins, M. A. Rahman, T. Zhu, Y. Sha, I. Manners and C. Tang, *ACS Macro Lett.*, 2019, **8**, 835; (*b*) J. Xu, H. Zhou, Q. Yu, G. Guerin, I. Manners and M. A. Winnik, *Chem. Sci.*, 2019, **10**, 2280; (*c*) S. Song, Q. Yu, H. Zhou, G. Hicks, H. Zhu, C. K. Rastogi, I. Manners and M. A. Winnik, *Chem. Sci.*, 2020, **11**, 4631; (*d*) H. Qiu, Y. Gao, C. E. Boott, O. E. Gould, R. L. Harniman, M. J. Miles, S. E. Webb, M. A. Winnik and I. Manners, *Science*, 2016, **352**, 697; (*e*) T. Xia, Z. Tong, Y. Xie, M. C. Arno, S. Lei, L. Xiao, J. Y. Rho, C. T. J. Ferguson, I. Manners, A. P. Dove and R. K. O'Reilly, *J. Am. Chem. Soc.*, 2023, **145**, 25274; (*f*) X. Zhang, G. Chen, L. Liu, L. Zhu and Z. Tong, *Macromolecules*, 2022, **55**, 8250; (*g*) M. C. Arno, M. Inam, Z. Coe, G. Cambridge, L. J. Macdougall, R. Keogh, A. P. Dove and R. K. O'Reilly, *J. Am. Chem. Soc.*, 2017, **139**, 16980; (*h*) M. A. H. Farmer, O. M. Musa and S. P. Armes, *J. Am. Chem. Soc.*, 2024, **146**, 16926; (*i*) J. Jiang, E. Nikbin, Y. Liu, S. Lei, G. Ye, J. Y. Howe, I. Manners and M. A. Winnik, *J. Am. Chem. Soc.*, 2023, **145**, 28096; (*j*) T. Xia, L. Xiao, K. Sun, J. Y. Rho, Y. Xie, S. J. Parkinson, L. Sangroniz, J. Zhang, J. Lin, A. J. Müller, L. Gao, A. P. Dove and R. K. O'Reilly, *Macromolecules*, 2024, **57**, 11210; (*k*) Z. Tong, Y. Xie, M. C. Arno, Y. Zhang, I. Manners, R. K. O'Reilly and A. P. Dove, *Nat. Chem.*, 2023, **15**, 824; (*l*) M. Inam, G. Cambridge, A. P. Barry, Z. P. L. Laker, N. R. Wilson, R. T. Mathers, A. P. Dove and R. K. O'Reilly, *Chem. Sci.*, 2017, **8**, 4223.

8 (*a*) S. Ogi, K. Sugiyasu, S. Manna, S. Samitsu and M. Takeuchi, *Nat. Chem.*, 2014, **6**, 188; (*b*) R. D. Mukhopadhyay and A. Ajayaghosh, *Science*, 2015, **349**, 241; (*c*) J. Kang, D. Miyajima, T. Mori, Y. Inoue, Y. Itoh and T. Aida, *Science*, 2015, **347**, 646; (*d*) W. Wagner, M. Wehner, V. Stepanenko, S. Ogi and F. Würthner, *Angew. Chem., Int. Ed.*, 2017, **56**, 16008; (*e*) S. Yagai, Y. Kitamoto, S. Datta and B. Adhikari, *Acc. Chem. Res.*, 2019, **52**, 1325; (*f*) G. Ghosh, S. Dey and S. Ghosh, *Chem. Commun.*, 2020, **56**, 6757; (*g*) B. Adelizzi, N. J. Van Zee, L. N. J. de Windt, A. R. A. Palmans and E. W. Meijer, *J. Am. Chem. Soc.*, 2019, **141**, 6110; (*h*) A. Sarkar, R. Sasmal, C. Empereur-mot, D. Bochicchio, S. V. K. Kompella, K. Sharma, S. Dhiman, B. Sundaram, S. S. Agasti, G. M. Pavan and S. J. George, *J. Am. Chem. Soc.*, 2020, **142**, 7606; (*i*) P. Khanra, A. K. Singh, L. Roy and A. Das, *J. Am. Chem. Soc.*, 2023, **145**, 5270; (*j*) H. Itabashi, K. Tashiro, S. Koshikawa, S. Datta and S. Yagai, *Chem. Commun.*, 2023, **59**, 7375; (*k*) H. Fu, J. Huang, J. J. B. van der Tol, L. Su, Y. Wang, S. Dey, P. Zijlstra, G. Fytas, G. Vantomme, P. Y. W. Dankers and E. W. Meijer, *Nature*, 2024, **626**, 1011; (*l*) N. Fujii, N. Hisano, T. Hirao, S. Kihara, K. Tanabe, M. Yoshida, S. Tate and T. Haino, *Angew. Chem., Int. Ed.*, 2025, **64**, e202416770.

9 (*a*) A. Rajak and A. Das, *Angew. Chem., Int. Ed.*, 2022, **61**, e20211657; (*b*) A. Rajak and A. Das, *Angew. Chem., Int. Ed.*, 2023, **62**, e2023142; (*c*) C. Chakraborty, A. Rajak and A. Das, *Nanoscale*, 2024, **16**, 13019.

10 (*a*) S. Lei, J. Tian, Y. Kang, Y. Zhang and I. Manners, *J. Am. Chem. Soc.*, 2022, **144**, 17630; (*b*) Y. Zhang, S. Pearce, J.-C. Eloi, R. L. Harniman, J. Tian, C. Cordoba, Y. Kang, T. Fukui, H. Qiu, A. Blackburn, R. M. Richardson and I. Manners, *J. Am. Chem. Soc.*, 2021, **143**, 5805; (*c*) R. Tao, H. Wang, R. Hou, B. Zheng, Y. Zhao, Y. Xie and Z. Tong, *Adv. Funct. Mater.*, 2025, 2500737.

11 (*a*) M. Clerc, S. Sandlass, O. Rifaie-Graham, J. A. Peterson, N. Bruns, J. R. de Alaniz and L. F. Boesel, *Chem. Soc. Rev.*, 2023, **52**, 8245; (*b*) H. M. D. Bandara and S. C. Burdette, *Chem. Soc. Rev.*, 2012, **41**, 1809; (*c*) D. R. S. Pooler, A. S. Lubbe, S. Crespi and B. L. Feringa, *Chem. Sci.*, 2021, **12**, 14964; (*d*) R. Klajn, *Chem. Soc. Rev.*, 2014, **43**, 148.

12 (*a*) J. K. Park and S. Lee, *J. Org. Chem.*, 2021, **86**, 13790; (*b*) Y. Rout, A. Ekbote and R. Misra, *J. Mater. Chem. C*, 2021, **9**, 7508; (*c*) D. Soni, S. Gangada, N. Duvva, T. K. Roy, S. Nimesh, G. Arya, L. Giribabu and R. Chitta, *New J. Chem.*, 2017, **41**, 5322.

13 S. Revoju, A. Matuhina, L. Canil, H. Salonen, A. Hiltunen, A. Abate and P. Vivo, *J. Mater. Chem. C*, 2020, **8**, 15486.

14 J. Rui, J. Pu, Z. Chen, H. Tang, L. Wang, S. J. Su and D. Cao, *J. Mater. Chem. C*, 2024, **12**, 9182.

15 (*a*) S. Gupta, A. K. Singh, R. K. Jain, R. Chandra and R. Prakash, *ChemElectroChem*, 2014, **1**, 793; (*b*) S. Gupta and R. Prakash, *J. Mater. Chem. C*, 2014, **2**, 6859; (*c*) E. Shiju, S. N. K. Narendran, N. D. Rao and K. Chandrasekharan, *New J. Chem.*, 2019, **43**, 7962; (*d*) X.-Q. Zhu, Z. Dai, A. Yu, S. Wu and J.-P. Cheng, *J. Phys. Chem. B*, 2008, **112**, 11694.

16 (*a*) Y. Zhu, L. Han, H. Fan, M. Wang, R. Qi, Y. Zhao and F. He, *Macromolecules*, 2020, **53**, 3217; (*b*) B. A. G. Lamers, B. Van Genabeek, J. Hennissen, B. F. M. De Waal, A. R. A. Palmans and E. W. Meijer, *Macromolecules*, 2019, **52**, 1200; (*c*) Y. Kwon and K. T. Kim, *Macromolecules*, 2021, **54**, 10487.

17 (*a*) D. Soni, S. Gangada, N. Duvva, T. K. Roy, S. Nimesh, G. Arya, L. Giribabu and R. Chitta, *New J. Chem.*, 2017, **41**, 5322; (*b*) D. Gil, B. Choi, J. J. Lee, H. Lee, K. T. Kim and C. Kim, *Ecotoxicol. Environ. Saf.*, 2023, **257**, 114954.

18 F. Liu, T. Wu, J. Cao, H. Zhang, M. Hu, S. Sun, F. Song, J. Fan, J. Wang and X. Peng, *Analyst*, 2013, **138**, 775.

19 J. C. Eloi, D. A. Rider, G. Cambridge, G. R. Whittell, M. A. Winnik and I. Manners, *J. Am. Chem. Soc.*, 2011, **133**, 8903.

20 (*a*) L. Luo, Y. Yang, S. Chen, P. Zhang and R. Zeng, *Molecules*, 2024, **29**, 614; (*b*) S. Wang, B. Zhang, W. Wang, G. Feng, D. Yuan and X. Zhang, *Chem.–Eur. J.*, 2018, **24**, 8157.

21 (*a*) Z. Zeng, H. Huang, Z. Fu, H. Lai, B. Long, A. Ali, T. Song and G. J. Deng, *Appl. Surf. Sci.*, 2021, **550**, 149361; (*b*) C. S. Barkschat, S. Stoycheva, M. Himmelhaus and T. J. J. Muller, *Chem. Mater.*, 2010, **22**, 52; (*c*) L. Carlinia, C. Fasolatob, P. Postorinob, l. Fratoddic, I. Vendittic, G. Testac and C. Battocchio, *Colloids Surf., A*, 2017, **532**, 183; (*d*) B. Pang, R. Köhler, V. Roddatis, H. Liu, X. Wang, W. Viöl and K. Zhang, *ACS Omega*, 2018, **3**, 6841.

22 (*a*) Z. M. Hudson, D. J. Lunn, M. A. Winnik and I. Manners, *Nat. Commun.*, 2014, **5**, 3372; (*b*) L. Xu, C. Wang, Y. X. Li, X. H. Xu, L. Zhou, N. Liu and Z. Q. Wu, *Angew. Chem., Int. Ed.*, 2020, **59**, 16675; (*c*) Q. Song, S. Goia, J. Yang, S. C. L. Hall, M. Staniforth, V. G. Stavros and S. Perrier, *J. Am. Chem. Soc.*, 2021, **143**, 382; (*d*) S. J. Zou, Y. Shen, F. M. Xie, J. De Chen, Y. Q. Li and J. X. Tang, *Mater. Chem. Front.*, 2020, **4**, 788.

23 (*a*) Z. Xie, Q. Huang, T. Yu, L. Wang, Z. Mao, W. Li, Z. Yang, Y. Zhang, S. Liu, J. Xu, Z. Chi and M. P. Aldred, *Adv. Funct. Mater.*, 2017, **27**, 1703918; (*b*) D. Tu, P. Leong, S. Guo, H. Yan, C. Lu and Q. Zhao, *Angew. Chem., Int. Ed.*, 2017, **56**, 11370; (*c*) H. Wang, Y. Li, Y. Zhang, J. Mei and J. Su, *Chem. Commun.*, 2019, **55**, 1879; (*d*) D. Li, W. Hu, J. Wang, Q. Zhang, X. M. Cao, X. Ma and H. Tian, *Chem. Sci.*, 2018, **9**, 5709.

24 (*a*) L. Wu, S. D. Bull, C. Huang, B. P. Emery, X. P. He, H. Tian, A. C. Sedgwick, J. Yoon, J. L. Sessler and T. D. James, *Chem. Soc. Rev.*, 2020, **49**, 5110; (*b*) A. Rajak, C. K. Karan, P. Theato and A. Das, *Polym. Chem.*, 2020, **11**, 695.

25 (*a*) H. Duman, F. Eker, E. Akdasçi, A. M. Witkowska, M. Bechelany and S. Karav, *Nanomaterials*, 2024, **14**, 1527; (*b*) W. J. Stark, P. R. Stoessel, W. Wohlleben and A. Hafner, *Chem. Soc. Rev.*, 2015, **44**, 5793; (*c*) D. V. Talapin and E. V. Shevchenko, *Chem. Rev.*, 2016, **116**, 10343.

26 (*a*) S. Mei, M. Staub and C. Y. Li, *Chem.–Eur. J.*, 2020, **26**, 349; (*b*) L. Jia, G. Zhao, W. Shi, N. Coombs, I. Gourevich, G. C. Walker, G. Guerin, I. Manners and M. A. Winnik, *Nat. Commun.*, 2014, **5**, 3882; (*c*) B. Dong, D. L. Miller and C. Y. Li, *J. Phys. Chem. Lett.*, 2012, **3**, 1346; (*d*) J. Tian, Y. Zhang, L. Du, Y. He, X. H. Jin, S. Pearce, J. C. Eloi, R. L. Harniman, D. Alibhai, R. Ye, D. L. Phillips and I. Manners, *Nat. Chem.*, 2020, **12**, 1150.

27 (*a*) J. B. Edel, A. A. Kornyshev, A. R. Kucernak and M. Urbakh, *Chem. Soc. Rev.*, 2016, **45**, 1581; (*b*) H. Han, J. Y. Lee and X. Lu, *Chem. Commun.*, 2013, **49**, 6122.

28 (*a*) M. Marchioni, C. Battocchio, Y. Joly, C. Gateau, S. Nappini, I. Pis, P. Delangle, I. M. Soret, A. Deniaud and G. Veronesi, *J. Phys. Chem. C*, 2020, **124**, 13467; (*b*) Y. Zhang, H. Peng, W. Huang, Y. Zhou, X. Zhang and D. Yan, *J. Phys. Chem. C*, 2008, **112**, 2330.

29 (*a*) S. Agnihotri, S. Mukherji and S. Mukherji, *RSC Adv.*, 2014, **4**, 3974; (*b*) Y. Wu, Y. Yang, Z. Zhang, Z. Wang, Y. Zhao and L. Sun, *Adv. Powder Technol.*, 2018, **29**, 407; (*c*) G. G. Flores-Rojas, F. L. Saucedo, E. Mendizábal and E. Bucio, *Polymers*, 2023, **15**, 125; (*d*) F. López-Saucedo, G. G. Flores-Rojas, J. López-Saucedo, B. Magariños, C. Alvarez-Lorenzo, A. Concheiro and E. Bucio, *Eur. Polym. J.*, 2018, **100**, 290.

30 (*a*) T. Iwata and Y. Doi, *Macromolecules*, 1998, **31**, 2461; (*b*) J. X. Zheng, H. Xiong, W. Y. Chen, K. Lee, R. M. V. Horn, R. P. Quirk, B. Lotz, E. L. Thomas, A.-C. Shi and S. Z. D. Cheng, *Macromolecules*, 2006, **39**, 641; (*c*) J. Yang, T. Zhao, Y. Zhou, L. Liu, G. Li, E. Zhou and X. Chen, *Macromolecules*, 2007, **40**, 2791; (*d*) M. Inam, G. Cambridge, A. P. Barry, Z. P. L. Laker, N. R. Wilson, R. T. Mathers, A. P. Dove and R. K. O'Reilly, *Chem. Sci.*, 2017, **8**, 4223; (*e*) X. He, Y. He, M. S. Hsiao, R. L. Harniman, S. Pearce, M. A. Winnik and I. Manners, *J. Am. Chem. Soc.*, 2017, **139**, 9221; (*f*) X. He, M. S. Hsiao, C. E. Boott, R. L. Harniman, A. Nazemi, X. Li, M. A. Winnik and I. Manners, *Nat. Mater.*, 2017, **16**, 481; (*g*) H. Qi, H. Zhou, Q. Tang, J. Y. Lee, Z. Fan, S. Kim, M. C. Staub, T. Zhou, S. Mei, L. Han, D. J. Pochan, H. Cheng, W. Hu and C. Y. Li, *Nat. Commun.*, 2018, **9**, 3005; (*h*) M. Inam, J. R. Jones, M. M. Pérez-Madrigal, M. C. Arno, A. P. Dove and R. K. O'Reilly, *ACS Cent. Sci.*, 2018, **4**, 63; (*i*) W. Yu, M. Inam, J. R. Jones, A. P. Dove and R. K. O'Reilly, *Polym. Chem.*, 2017, **8**, 5504; (*j*) M. L. Di Lorenzo and R. Androsch, *Polym. Int.*, 2019, **68**, 320; (*k*) Z. Li, Y. Zhang, L. Wu, W. Yu, T. R. Wilks, A. P. Dove, H. Ding, R. K. O'Reilly, G. Chen and M. Jiang, *ACS Macro Lett.*, 2019, **8**, 596; (*l*) P. J. Hurst, A. M. Rakowski and J. P. Patterson, *Nat. Commun.*, 2020, **11**, 4690; (*m*) G. Virata and E. B. Gowd, *Polym. Chem.*, 2022, **13**, 838.

31 (*a*) C. Battocchio, F. Porcaro, S. Mukherjee, E. Magnano, S. Nappini, l. Fratoddi, M. Quintiliani, M. V. Russo and G. Polzonetti, *J. Phys. Chem. C*, 2014, **118**, 8159; (*b*) R. Sharma, A. Dhillon and D. Kumar, *Sci. Rep.*, 2018, **8**, 5189.

32 (*a*) W. Ali, V. Shabani, M. Linke, S. Sayin, B. Gebert, S. Altinpinar, M. Hildebrandt, J. S. Gutmann and T. M. Gall, *RSC Adv.*, 2019, **9**, 4553; (*b*) J. M. Mativetsky, Y. L. Loo and P. Samorì, *J. Mater. Chem. C*, 2014, **2**, 3118.